Physics of the Earth and Planetary Interiors 280 (2018) 40–52

Contents lists available at ScienceDirect

Physics of the Earth and Planetary Interiors

journal homepage: www.elsevier.com/locate/pepi

A continuous Late Holocene paleosecular variation record from Carmen Lake (Tierra del Fuego, Argentina)

Claudia S.G. Gogorza[a,*], María A. Irurzun[a], María J. Orgeira[b], Pedro Palermo[a], María Llera[b]

[a] Centro de Investigaciones en Física e Ingeniería del Centro de la Provincia de Buenos Aires (CIFICEN – CONICET – UNCPBA – CICPBA), Tandil, Argentina
[b] Instituto de Geociencias Básicas, Aplicadas y Ambientales de Bs. As (IGEBA-CONICET), Universidad de Buenos Aires, Buenos Aires, Argentina

ARTICLE INFO

Keywords:
Paleomagnetism
Secular variations
Late Holocene
Lake sediments
Argentina

ABSTRACT

Paleomagnetic secular variations (PSV) give us information on the mechanisms of the geodynamo and can also be used for stratigraphic correlation on a regional scale. In this article we present a high-resolution paleomagnetic and rock magnetic study of two cores, LCTF1 and LCTF2, collected at Carmen Lake (Tierra del Fuego, Argentina). An analysis of rock magnetic data suggests that the remanence signal is carried by Titanomagnetite grains in stable pseudo single domain (PSD) state. Notwithstanding the special mechanism of sedimentary deposition, the sequence is characterised by good paleomagnetic properties and can be used to reconstruct a continuous stratigraphic record that provides high-resolution declination, inclination and relative paleointensity curves for the period 1000–4000 cal years BP. The constructed PSV curves are in very good agreement with the available records of Southern Argentina, implying very promising results in the construction of curve patterns for the region. A comparison of the records of southern Argentina with the most recent models available demonstrates that there is a noticeable lack of agreement, which is interpreted as the critical need to add more data from the southern hemisphere in the construction of the geomagnetic field models.

1. Introduction

It has been known for over 300 years, since the discovery by Gellibrand in 1635 that the geomagnetic field changes over time. He noted that whereas Borough in 1580 had measured a value of 11.3°E for the declination in London, his own measurements in 1634 yielded only 4.1°E. The difference was far greater than possible experimental error. The gradual change in magnetic field over time is called the secular variation and is observed in all the magnetic elements (Merrill and Mc Elhinny, 1983). Variations in the geomagnetic field observed on the earth's surface occur on time scales ranging from milliseconds to millions of years. These sources have different physical origins and can be found both below (in the form of electrical currents and magnetised material) and above (only in the form of electrical currents) the Earth's surface (Olsen et al., 2010). Paleomagnetic studies performed on sedimentary sequences are being carried out worldwide to establish high resolution paleosecular variation records (Nourgaliev et al., 2003; Bleil and Dillon, 2008; Stoner et al., 2007; Yang et al., 2012; Gogorza et al., 2012; Lisé-Pronovost et al., 2013; Usapkar et al., 2016; to cite some of the latest papers), which can be used to correlate regional stratigraphies (Frank et al., 2002; Holme and Olsen, 2006; Barletta et al., 2010), determine the sediment ages effectively, and understand the temporal characteristics of the geodynamo of the Earth's magnetic field (Anker et al., 2001; St-Onge et al., 2003; Lisé-Pronovost et al., 2013; Yang et al., 2013). Paleosecular variation studies are therefore a fundamental source of information for a deeper understanding of the natural variability of the geomagnetic field and for the modelling of the geodynamo processes and outer core's fluid dynamics. For the latter it is necessary to have overall data distribution. In particular, one of the regions in the world with strikingly poor data coverage is the Southern Hemisphere (Korte and Constable, 2011). A major limitation to the collection of high-resolution records from this vast region is the scarcity of adequately high sedimentation rate basins and their accessibility (Lisé-Pronovost et al., 2013). Despite this, a series of Pleistocene-Holocene records have been obtained in the last decade (Gogorza et al., 2011, 2012; Lisé-Pronovost et al., 2013; to cite some of the latest papers).

Sediments are attractive recorders of the geomagnetic field due to their continuity, high temporal resolution, and global availability. Taking this into account and in order to add data on this poorly covered region, we present the records corresponding to Carmen Lake, northern Tierra del Fuego (Argentina) and describe a paleomagnetic and rock magnetic study of two piston cores recovered in the Austral Autumn of 2011. Sedimentation rates in the sedimentary cores are about 0.3 mm/year, which implies that these lake sediments may record geomagnetic

* Corresponding author.
E-mail address: claudiagogorza65@gmail.com (C.S.G. Gogorza).

https://doi.org/10.1016/j.pepi.2018.04.006
Received 1 November 2017; Received in revised form 13 April 2018; Accepted 18 April 2018
Available online 24 April 2018

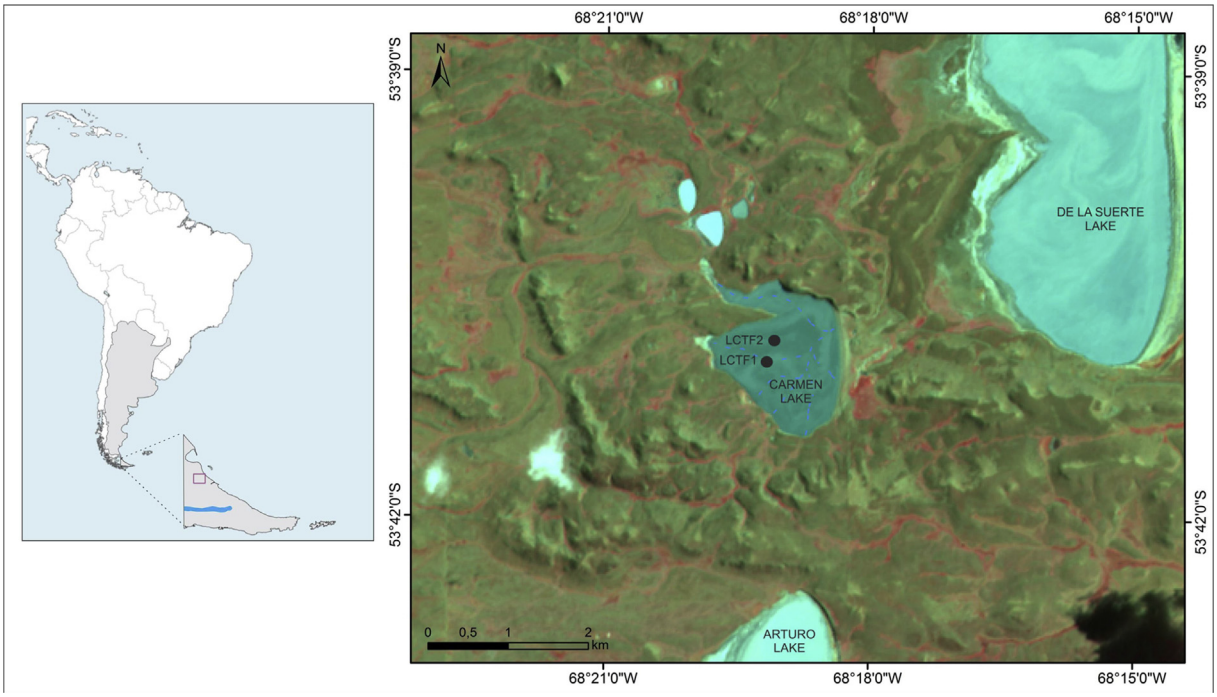

Fig. 1. Location maps: (a) Geographical location of Carmen Lake, (b) Locations of the piston coring sites.

features with wavelengths of the order of a few hundred years, thus providing temporal and spatial descriptions of the paleomagnetic field at high latitude.

2. Location of the cores and sampling

Carmen Lake (53°40′S 68°18′W) is a shallow water body fed by short and temporary water streams with pluvio-nival regime, located 29 m a.s.l. (Fig. 1). Its form is sub-circular, with a rectilinear extension of 1 km in N-W direction. The major axis is 1.74 km in N-S direction while the minor axis is 1.62 km in W-E direction. It has a perimeter of 7.13 km and an area of 1.97 km^2. It is the depocenter of a closed basin located in a mountain system with strong fluvial dissection and general slope towards the NE (Coronato et al., 2017).

Two short cores (LCTF1 and LCTF2, 115 and 117 cm long, respectively) were collected using a Livingstone piston corer during the Austral Autumn of 2011 at a depth of 1.5 m below lake water surface (b.l.w.s.) and at some metres distance from each other (Fig. 1). Sediments were cored into plastic tubes, of 60 mm in inner diameter and stored in cold, dark and dry conditions at the Laboratory of Research on Continental and Marine Environments, a laboratory of the Institute of Andean Studies “Don Pablo Gröeber”, Buenos Aires University. After dividing the cores into working and archive halves, each core section was sub-sampled for paleomagnetic and rock magnetic measurements at the lab. Both cores were photographed and described lithologically.

3. Sedimentological studies

Sedimentological studies show that the LCTF1 and LCTF2 sediment cores are composed mainly of massive silt with thin layers of silty sand (see lithologic log in Fig. 2, modified from Coronato et al. (2017)). The main characteristics of the studied units are described below:

LCTF1 core:

Unit c (115–55 cm) contains silt (73–82%) with low proportions of clay (10–18%) and fine sand (6–7%). It includes several layers of sandy silt composed of silt (56–58%), fine sand (36–38%) with low proportions of clay (1–3%). The thickness of the layers varies between 0.1 and 4 cm. A sandstone fragment is observed at 73 cm depth (Fig. 2). The organic matter contained in a sample taken from the bottom of this Unit, dated with the accelerator mass spectrometer (AMS) radiocarbon method, has indicated an age of 3300 ± 30 years BP (^{14}C years before present) (Table 1, Fig. 2).

Unit b (55–10 cm) is characterised by sandy silt composed of silt (71%) and fine to very fine sand (22%) with low proportions of clay (6%). This sub-unit contains some more sandy lenses, with high proportions of mainly medium-fine sand (46%) and low proportion of coarse sand (2%). These sandy silt layers are concentrated between 40 and 30 cm and they disappear along the upper 20 cm of the subunit. The upper section contains gray mottle. The organic matter contained in a sample taken at 10 cm depth, dated with the AMS radiocarbon method, has indicated an age of 1220 ± 30 years BP (Table 1, Fig. 2).

Unit a (10–0 cm) is composed mainly of silt (79%) and clay (14%), with low content of fine sand (6%). It appears disturbed and its colour varies between G1/3/5GY and 2.5Y/5/3.

LCTF 2 core:

In Unit c (117–51 cm), sandy layers and sandy lenses are composed of silt (53%) and fine sand (39%) with low proportion of clay (7%). In general, the thickness of the sandy layers varies between 0.1 and 1 cm. However, a 5 cm thick sandy layer is observed towards the top of the sub-unit. The resulting ages for the base and the top of this sub-unit yielded by two organic matter samples dated with the AMS radiocarbon method, are 3616 ± 29 years BP and 2141 ± 21 years BP, respectively (Table 1, Fig. 2).

Unit b (51–16 cm) is characterised by the absence of sandy layers in the lower part (51–31 cm), which appear between 30 and 20 cm, towards the upper part. The layers have a maximum thickness of 1 cm. A sandstone fragment is observed around 30 cm-depth (Fig. 2). The organic matter contained in a sample taken at 16.5 cm depth, dated with the AMS radiocarbon method, has indicated an age of 1544 ± 27 years BP (Table 1, Fig. 2).

Unit a (16–0 cm) is 2.5Y/3/2 in colour with 2.5y/3/2 coloured layers (Fig. 2). These layers are composed of silt (79%) and clay (14%) with low content of fine sand (6%). The sub-unit includes 0.5 cm-thick sandy layers. It is not possible to clearly correlate this unit in both cores because the top 11 cm of LCTF1 is disturbed.

Taking into account both cores, the lithology of the geological

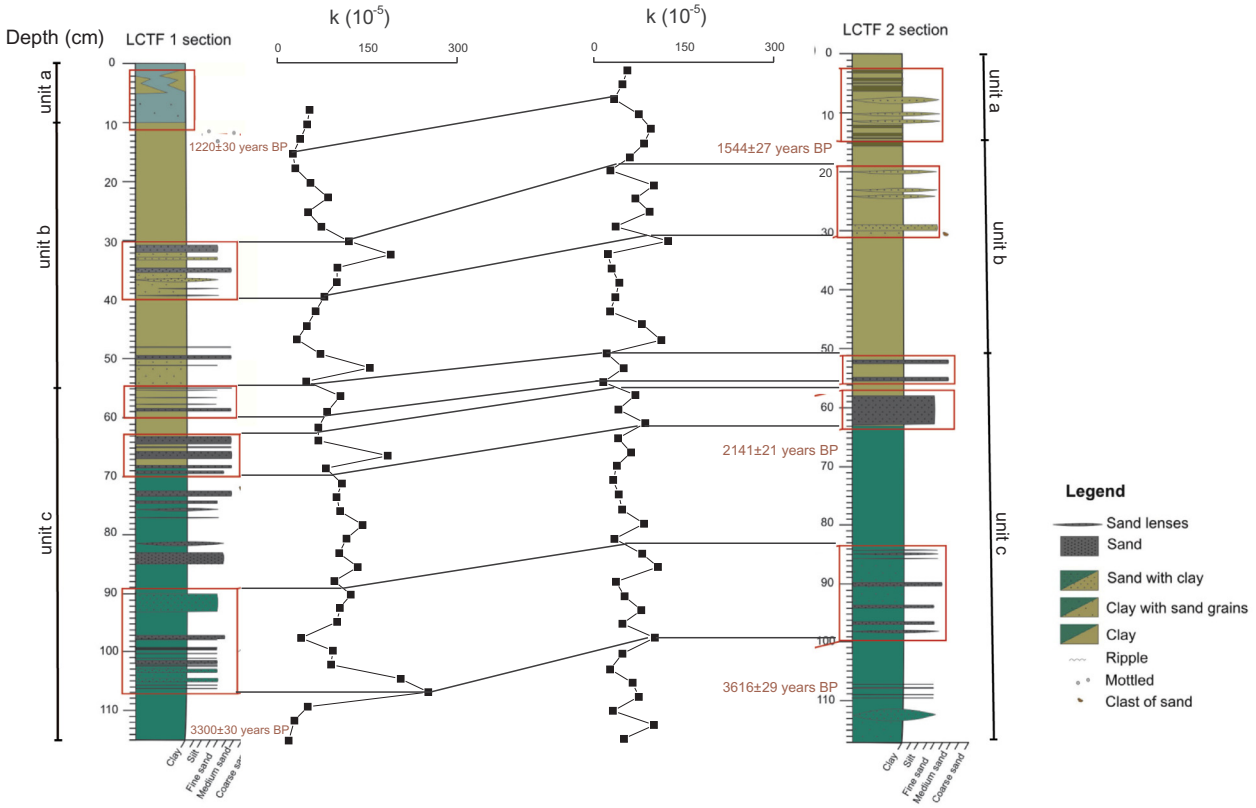

Fig. 2. Sedimentology description and correlation of magnetic susceptibility (k) profiles of cores LCTF1 and LCTF2. Radiocarbon dates are indicated with red text. (For interpretation of the references to colour in this figure legend, the reader is referred to the web version of this article.)

Table 1
Radiocarbon age determinations and calibrated age ranges. Calibration was calculated using the Oxcal 4.2 calibration software (Bronk Ramsey, 2008; Bronk Ramsey and Lee, 2013).

Sample	Material	Lab Code	Depth (cm)	^{14}C age (years BP)	Median cal age (cal years BP)	Maximum (2σ BP)	Minimum (2σ BP)
LCTF1-14	Organic matter	Beta-343218	14	1220 ± 30	1087	1109	1056
LCTF1-113	Organic matter	Beta-343219	113	3300 ± 30	3485	3512	3447
LCTF2-16.5	Organic matter	AA104695	16.5	1544 ± 27	1379	1411	1353
LCTF2-65.7	Organic matter	AA107270	65.7	2141 ± 21	2071	2116	2010
LCTF2-109	Organic matter	AA104696	109	3616 ± 29	3875	3923	3832

record is consistent with conditions of continuous subaqueous sedimentation, with no geological or geochemical evidences of desiccation events. The association between the described sedimentological lithofacies and ostracod species, typical of diluted waters, suggests a positive hydrological balance maintained by discharge of the lake's tributaries. Along the geological record, several sedimentary structures demonstrate the influence of episodic tractive currents in the water body (Laprida et al., in preparation).

The lithological correlation between cores was performed with very general lines. Although the lithological units described in Coronato et al. (2017) may be fairly environmentally correlated, the presence of numerous tributaries in the lake with different sedimentary source areas (and therefore different sediment loads associated with runoff) obscures the correlation from bed to bed. Thus, both cores have been under the influence of the sedimentary input of different lake tributaries during the lapse comprised by the sedimentological record.

4. Methodology

Paleomagnetic and rock magnetic measurements were performed at the laboratory of Paleomagnetism and Environmental Magnetism in Tandil (Buenos Aires, Argentina). Cubic plastic boxes (8 cm^3) were pushed into the split core faces in such a way that the samples were taken one next to the other (n = 45 for LCTF1 and n = 48 for LCTF2), and were removed with a plastic spatula. Magnetic susceptibility was measured at low and high frequencies using a Bartington MS2 magnetic susceptibility meter at 0.47 kHz (k_{low}) and 4.7 kHz (k_{high}), respectively. The frequency dependence factor (F) was calculated from the difference between measurements at high and low frequencies, i.e., $F = (k_{low} - k_{high})/k_{low}$. This parameter reveals the presence of very fine (< 0.03 μm for magnetite) ferrimagnetic grains in the super-paramagnetic state (SP) of the sediment record (Dearing, 1999). The natural remanent magnetisation (NRM, D and I) was measured using a JR6A Dual Speed Spinner Magnetometer. One sample every four was subjected to stepwise alternating field (AF) demagnetisation using fourteen steps up to 100 mT. The analysis of demagnetisation results of pilot samples suggests that the viscous component of NRM can be removed by applying 10 mT demagnetisation field. Therefore, the remaining samples were progressively AF-demagnetised from 0 to 50 mT in steps of 10 mT, and characteristic remanent magnetisation (ChRM), i.e., paleomagnetic inclination, declination and intensity as well as the maximum angle of deviation (MAD), were calculated by using Principal Component Analysis (PCA, Kirschvink, 1980). After the measurement of NRM, an anhysteretic remanent magnetisation (ARM) was applied

along the z-axis with a peak alternating field of 100 mT and a steady bias field of 50 μT. The Isothermal Remanent Magnetisation (IRM) was acquired at room temperature in increasing steps up to 2 T reaching saturation (SIRM), with an IM-10-30 Pulse Magnetiser (ASC Scientific). Subsequently, AF demagnetisations of the ARM and SIRM, respectively, were measured using the same steps as for the NRM demagnetisation. Different magnetic properties and inter-parametric ratios were used to determine down-core variations in the type, concentration, and grain size of magnetic minerals. Magnetic susceptibility was used as a first-order indicator of the concentration of magnetic (*sensu lato*) minerals. S-ratio was calculated using the formula S-ratio = IRM_{-300mT}/IRM_{2T} (Thompson and Oldfield, 1986; Bloemendal et al., 1988). Combined magnetic parameters were calculated (SIRM/k and ARM/SIRM). In addition, and as a first estimate of relative magnetic grain-size variations, the median destructive field of the NRM (MDF_{NRM}) was determined. Susceptibility vs. temperature measurements (k-T curves) under air were carried out using a Bartington susceptibility meter equipped with furnace. The pilot samples were heated up to about 700 °C at a heating rate of 20 °C/min and then cooled at the same rate. Hysteresis loops were measured in fields up to maximum of 1 T using a Molspin VSM (Vibration Sample Magnetometer) at the Institute of Basic, Applied and Environmental Geosciences of Buenos Aires (IGEBA; Buenos Aires, Argentina) to find out the domain state of the magnetic minerals (Day et al., 1977; Dunlop, 2002).

5. Results

5.1. Core correlation

The correlation of susceptibility records of both cores is not obvious at first sight (Fig. 2). This is due to the characteristic of the sedimentological record as was mentioned above. Both cores were under the influence of different lake tributaries. As a consequence, different variations in grain size due to the input of tractive currents are expected for each one. Consequently, such variations significantly affect the magnetic susceptibility. Despite this, studies of magnetic properties, shown later in this contribution, indicate that there is no significant variation in magnetic mineralogy. After careful visual examination of the sediments, good correlation can be achieved (Fig. 2). Susceptibility logs were used to define tie-lines for the lithostratigraphic correlation of cores. These tie-lines are consistent with lithology.

5.2. Rock magnetism

5.2.1. Magnetic concentration

The magnetic parameters k, NRM, ARM and SIRM are mainly related to the concentration and type of magnetic minerals, but they differ in their sensitivity to variations in magnetic grain size. While ARM is sensitive to single domain (SD) and pseudo-single domain (PSD) grains, k and SIRM are also sensitive to coarser grain sizes of magnetic minerals mainly in the multidomain (MD) state (Bailey and Dunlop, 1983; Thompson and Oldfield, 1986). NRM may also reflect the strength of the geomagnetic field when the remanence was acquired. All rock-forming minerals contribute to k in proportion to their relative abundance and specific magnetic susceptibility, so that the measured k value can be biased by diamagnetic and paramagnetic contributions, if the concentration of ferrimagnetic minerals is low.

In order to better compare the rock magnetic parameters of both cores, they were plotted using the same depth-scale after the process of correlation. Fig. 3 shows the down-core stratigraphic trends of the remanence parameters measured for LCTF1 and LCTF2 cores. The linear correlation among them indicates that the variations of these parameters are dominantly controlled by concentration of magnetic minerals (Moreno et al., 2002). Oscillations of the magnetic susceptibility and of the NRM, ARM and SIRM intensities throughout the cores are limited, with values comprised within the same order of magnitude, except for samples 41 (95.9 cm) and 42 (98.3 cm) of LCTF1, whose values of k are much higher than those of the remaining samples (191.5 and 233.9×10^{-5}, respectively). In particular, k fluctuates around a mean value of 84.4×10^{-5} in LCTF1 and 57.7×10^{-5} in LCTF2 (with a full range of variability from ca. 18.1×10^{-5} to 233.9×10^{-5} and 18.9×10^{-5} to 116.8×10^{-5}, respectively), with few sharp peaks, which are linked to sand layers and/or sand lenses. NRM ranges around a mean value of 17.4 mA/m in LCTF1 and 17.8 mA/m in LCTF2 (with a full range of variability from 4.7 mA/m to 37.6 mA/m and 7.4 to 36.1 mA/m, respectively). ARM mostly oscillates around a mean value of 96.3 mA/m in LCTF1 and 82.8 mA/m in LCTF2 (with a full range of variability from 40.8 mA/m to 158.9 mA/m and 31.6 to 140.1 mA/m, respectively). Finally, SIRM varies around a mean value of 5680.4 mA/m in LCTF1 and 4339.5 mA/m in LCTF2 (with a full range of variability from 1480.9 mA/m to 12133.8 mA/m and 1654.2 mA/m to 8463.7 mA/m, respectively).

When comparing the concentration-dependent parameters profiles of both cores, we can see, in general, that the records of LCTF1 show higher values than those of LCTF2, especially in the lower half, which could be associated with higher contribution of magnetic minerals in this section. Moreover, the observed lack of coherence of k with remanence parameters between 100 and 95 cm in LCTF1would indicate the possible occurrence of a relatively higher proportion of coarser magnetic grain size and/or paramagnetic contributions in this interval. All the apparent discrepancies of magnetic parameters between both cores, mentioned in the paragraphs above, are explained in terms of the mechanics of sedimentary deposition. Different input in the cores due to the influence of different lake tributaries generates different concentrations of magnetic minerals in both cores, as well as variations in the magnetic particle size.

5.2.2. Magnetic mineralogy

The S-ratio is linked to magnetic mineralogy. Consistent with previous studies in southern Patagonia (Gogorza et al., 2011, 2012; Lisé-Pronovost et al., 2013), our results indicate that low-coercivity mineral (probably magnetite) is the dominant magnetic mineral. The S-ratio remains remarkably constant and varies around 0.94 in LCTF1 and LCTF2 (with a full range of variability from 0.93 to 0.96 and 0.9 to 0.97, respectively) (Fig. 4), which is indicative of the predominance of low-coercivity grains. Both records show a very good agreement, except for slight differences in the interval 61.6–54.6 cm, when LCTF1 shows a decrease in the content of soft magnetic grains. The average value of the MDF_{NRM} (not shown) and the coercive force (Bc; not shown) is about 23 mT and 5 mT for LCTF1 and about 21 mT and 4.5 mT for LCTF2, respectively. Along with the typical shape of the hysteresis loop (Fig. 5a) (Tauxe et al., 1996), these results are characteristic of magnetite.

Stepwise acquisition of isothermal remanent magnetisation (IRM) in fields of up to 2 T supports that more than 90% of SIRM was acquired in fields between 150 and 200 mT (Fig. 5b). This indicates that low-coercivity minerals are the dominant magnetic carriers. Progressive removal of SIRM by back-field demagnetisation indicates that coercivities (Bcr) vary between 28 and 38 mT (32.2 ± 0.3 mT) and between 30 and 39 mT (33.8 ± 0.3 mT) for LCTF1 and LCTF2, respectively, which is typical of magnetite (e.g., Dunlop and Özdemir, 1997). In this case, in which the magnetic mineralogy is dominated by magnetite, the best way to assess variations in concentration is by means of the bilogarithmic plot of k vs. SIRM (Fig. 5c), which was calibrated according to Thompson and Oldfield (1986). From this relationship, we estimated that the concentration of ferrimagnetic minerals varies approximately between 0.01% and 0.09%.

Thermomagnetic curves obtained for a set of pilot samples (only one is shown in Fig. 5d), with their nearly reversible behaviour, indicate the presence of two magnetic phases. Both Curie temperatures, 210 ± 20 °C and 522 ± 50 °C in the heating curve and 280 ± 24 °C and 506 ± 20 °C in the cooling curve, were obtained using the method

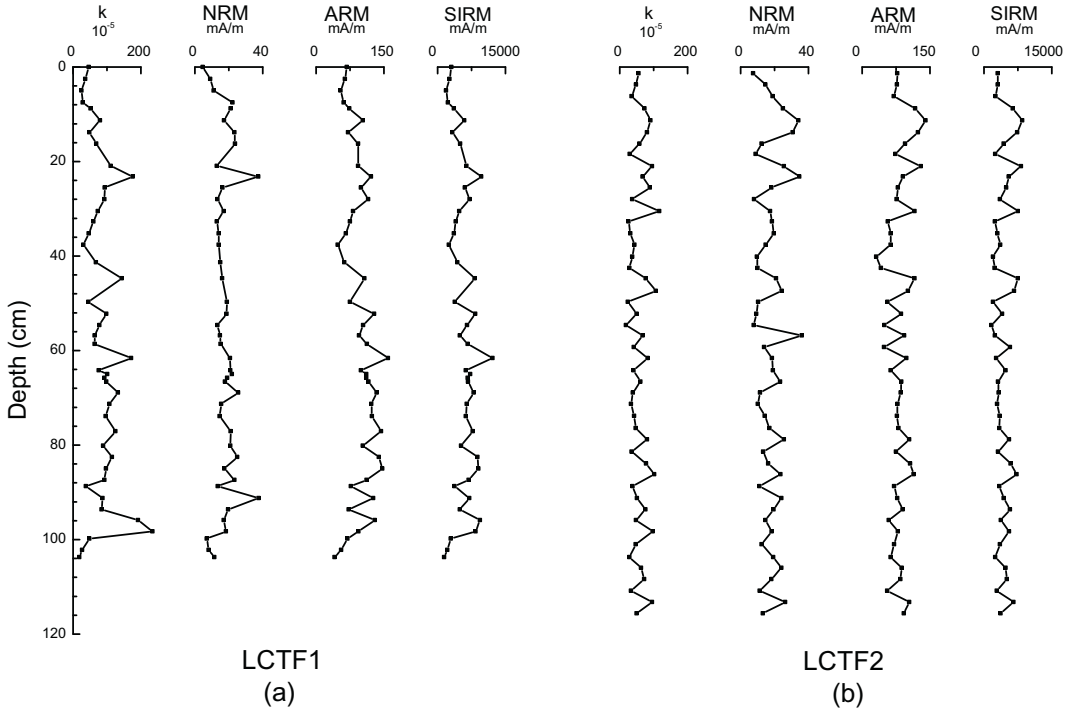

Fig. 3. Down-core variations in concentration-magnetic parameters: magnetic susceptibility (k), NRM, ARM and SIRM of cores LCTF1 (a) and LCTF2 (b).

proposed by Prévot et al. (1983). The low temperature phase is typical of Titanomagnetite (Dunlop and Özdemir, 1997) and the shift to a high Curie temperature in the cooling curve is also expected for this type of mineral (Lattard et al., 2006). The high temperature phase corresponds to Ti-low Titanomagnetite (Dunlop and Özdemir, 1997), and the difference in the temperatures between heating and cooling curves is within the error tolerance. The small irreversibility could be interpreted as limited neo-formation of magnetite or loss of Ti upon heating. These results are consistent with the presence of Titanomagnetite as the main ferromagnetic carrier.

5.2.3. *Magnetic grain size*

SIRM/k ratio is consistent with a magnetic grain size of app. 8–16 μm (Fig. 5c). The linearity of the SIRM/k implies that the grain size does not change much within the sediments (except in the interval 66.6–54.6 cm). The inter-parametric ratios ARM/SIRM and SIRM/k are considered potential magneto-granulometric indicators, with higher values for finer grained (SD) ferrimagnetic particles and lower values

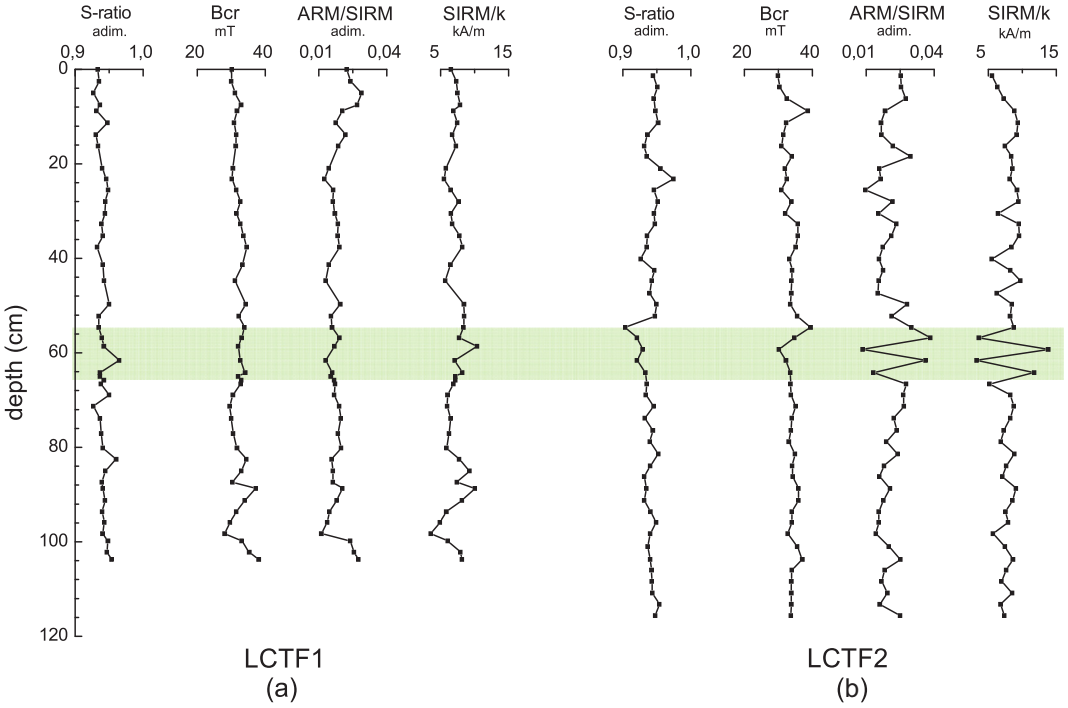

Fig. 4. Rock magnetic studies: S-ratio, Bcr, ARM/SIRM and SIRM/k of cores LCTF1 (a) and LCTF2 (b).

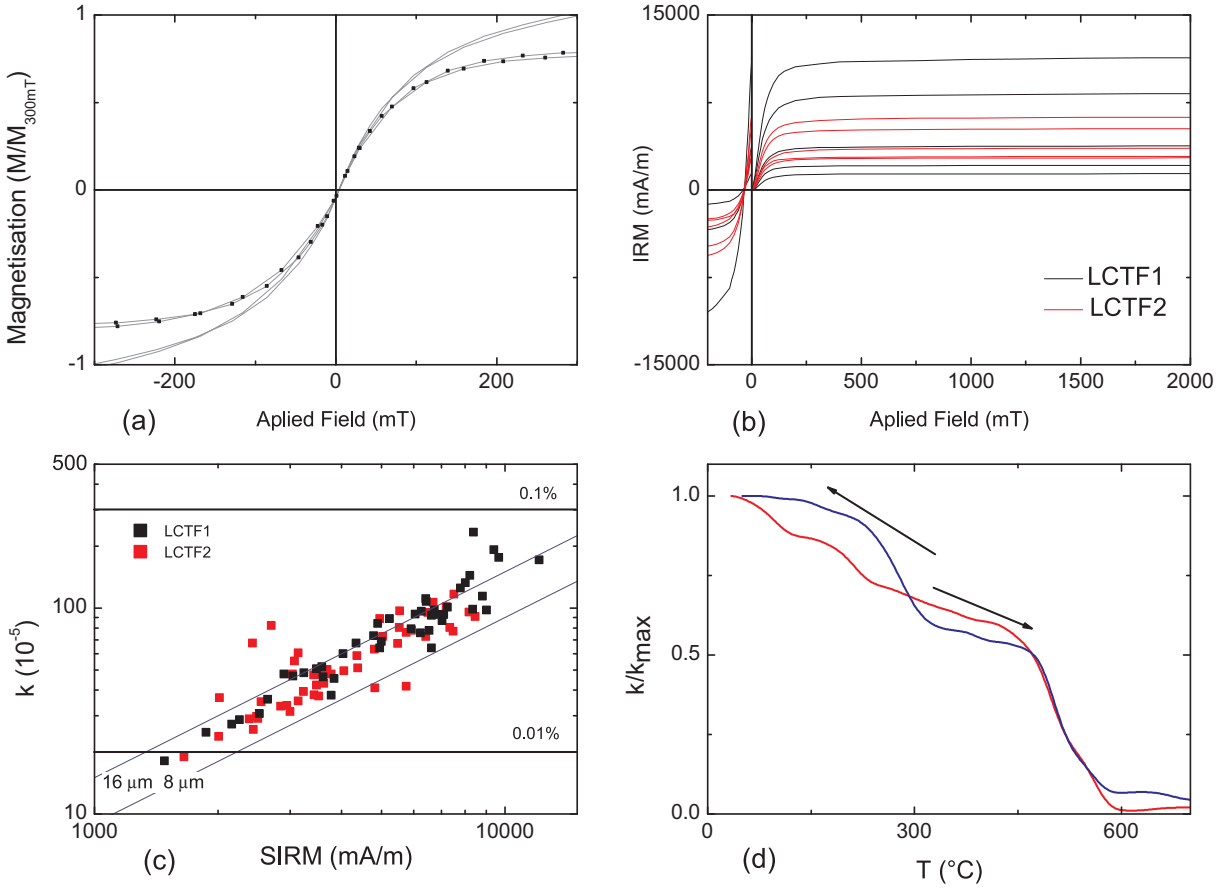

Fig. 5. Rock magnetic properties of the Carmen Lake sediments. (a) Hysteresis curve for a typical sample. The raw (gray) and high-field slope corrected (black) magnetisation are illustrated, (b) Isothermal Remanent Magnetisation (IRM) acquisition curves, for representative samples from cores LCTF1 and LCTF2 (c) Susceptibility (k) versus Saturation of the Isothermal Remanent Magnetisation (SIRM) for all samples in order to estimate concentration and grain size, according to Thompson and Oldfield (1986) and (d) Susceptibility vs. temperature measurements of a pilot sample.

for larger (MD) grains. Grain-size interpretations based on these ratios assume that k, ARM, and IRM reflect the same ferrimagnetic minerals. This assumption is commonly violated when k is significantly affected by paramagnetic and/or diamagnetic material, when IRM contains a large hematite component, and when there are major changes in ferrimagnetic minerals (Heil et al., 2009; Thompson and Oldfield, 1986; Evans and Heller, 2003. ARM/SIRM and SIRM/k ratios suggest that the behaviour of the magnetic grain size is quite similar and rather uniform in both cores, except in the interval 66.6–54.6 cm, where the magnetic input grain size underwent rapid and abrupt changes in LCTF2 (Fig. 4). This behaviour would be related to the difference in the contribution of paramagnetic minerals and variations in the layers of both cores (such as sand lenses). It is necessary to be cautious in the analysis of the magnetic grain size-dependent parameters when studying cores with different contributions of paramagnetic minerals. In these cases, the most appropriate interpretation is based on the remanence parameters (ARM/SIRM).

Hysteresis parameters (Fig. 6) reveal that the magnetite grains are in the pseudo-single domain range (Day et al., 1977; Dunlop, 2002). Analysing the small group of samples (6 samples) that fall in the top part of the Day Plot, we see they are samples with very low values of k and NRM located at the top of the LCTF1 (Fig. 3), then we link this behaviour with errors associated with the measurements rather than the presence of SP particles. F values (not shown) are, for the majority of the samples < 0.03, indicating none or minor contributions from SP particles. Besides, the environmental conditions of the lake, as well as of the soils of the adjacent areas, make practically impossible the existence of suitable conditions for organic (via anaerobic bacteria) or inorganic formation of SP particles. However, a small contribution of SP particles, which can lead to the displacement of these samples in the Day Plot to the SD + SP region, should not be excluded. The contribution of SP particles might have resulted from inclusions in volcanic glasses (Laprida et al., in preparation).

5.3. Dating

Five samples of organic matter were selected from cores LCTF1 and LCTF2 for radiocarbon dating (Table 1, Fig. 2). Radiocarbon datings were made by AMS at the Arizona Laboratory Facility (Arizona University, USA) and at the Beta Analytic Inc. Fig. 7 shows a plot of calibrated ages vs. depth. Ages were calibrated (Table 1) with the help of the OxCal program (Bronk Ramsey, 1995). These radiocarbon data allow the development of a time-scale by linear interpolation between data points. They were used together with remarkable features of down-core magnetic parameters variations (Fig. 2) for core correlation and construction of a composite core data set. An age-depth model (Fig. 7) was calculated with the Oxcal 4.2 (2017) calibration software (Bronk Ramsey, 2008; Bronk Ramsey and Lee, 2013). The stars are the dated and calibrated samples. As can be noted for the period between two stars, the further away from the dated samples, the greater the error obtained for that period. In this way the dating errors vary from 29 to 163 years.

5.4. Paleomagnetic record

Typical examples of vector endpoint diagrams during progressive

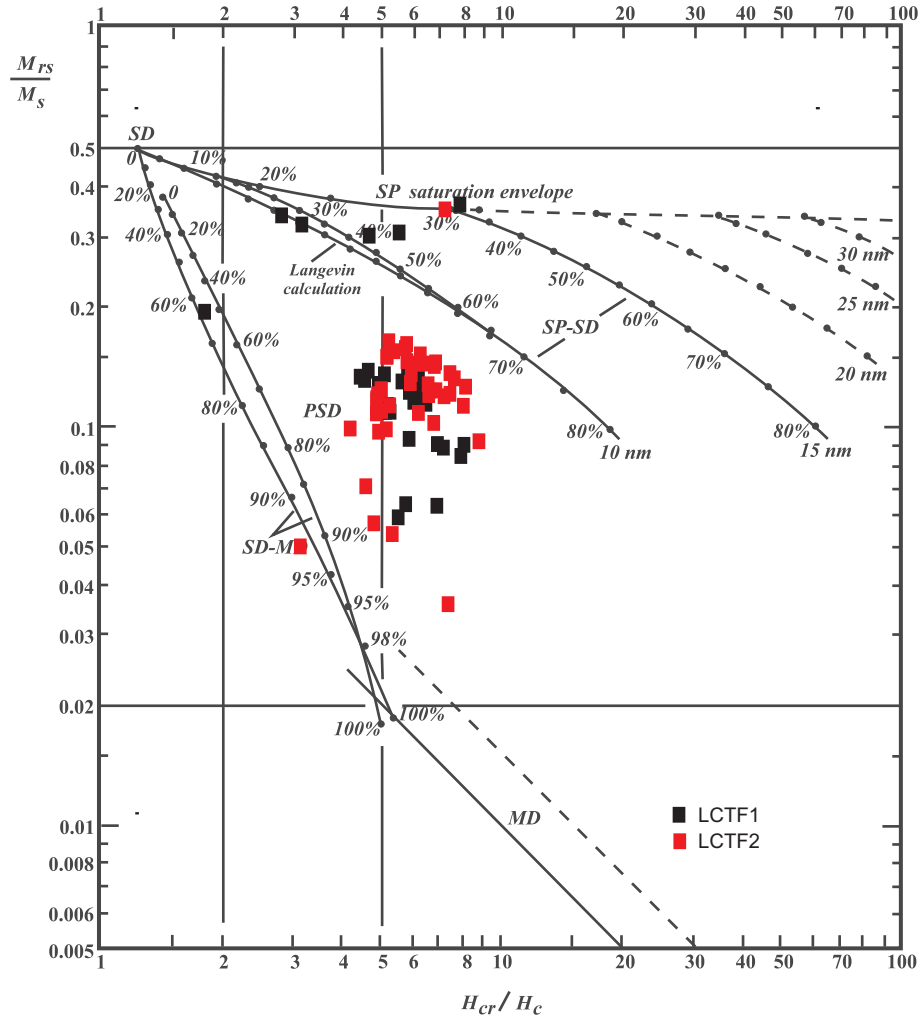

Fig. 6. Day plot (Day et al., 1977) for the sediment samples of Carmen Lake. The mixing reference lines are from Dunlop (2002).

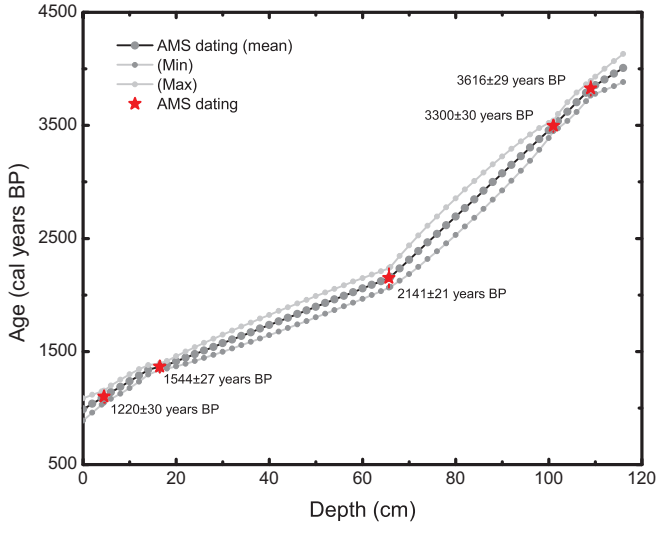

Fig. 7. Age-depth model of the composite profile and age errors (2σ) are shown by the data symbol (gray circles). Radiocarbon dates are indicated (red stars). (For interpretation of the references to colour in this figure legend, the reader is referred to the web version of this article.)

AF demagnetisation show a stable primary remanence pointing toward the origin after demagnetisation up to 100 mT (Fig. 8). Paleomagnetic directions were calculated by fitting a linear regression line to minimise the MAD. These values are generally smaller than 5°, attesting that the paleomagnetic directions are stable and well determined.

The mean inclination is −64.7° for core LCTF1 and −62.3° for core LCTF2 (Fig. 9); inclinations range between −51.9° and −78.9° and between −44.7° and −81.9°, respectively. The mean paleomagnetic inclinations for both cores are slightly shallower than the expected inclination at the studied site (−69.8°) for a geocentric axial dipole (GAD) field. Cores LCTF1 and LCTF2 are azimuthally unoriented and thus no absolute declination values could be obtained. We plot relative declinations centred on the mean declination for each core. Trends in inclination and declination of both cores are similar, although in the case of declination, the amplitude of certain features varies from one core to the other.

The final inclination and declination records for both cores and the stacked profile of arithmetic averages are plotted versus age in Fig. 9. The stacking removes spurious data exhibited by individual records and enhances the signal-to-noise ratio (Gogorza et al., 2011). Hence, the stacked record is often found to show fewer details than individual records (Creer and Tucholka, 1982). Inclination displays a decreasing trend from 4000 cal years BP to 2600 cal years BP, showing a notable

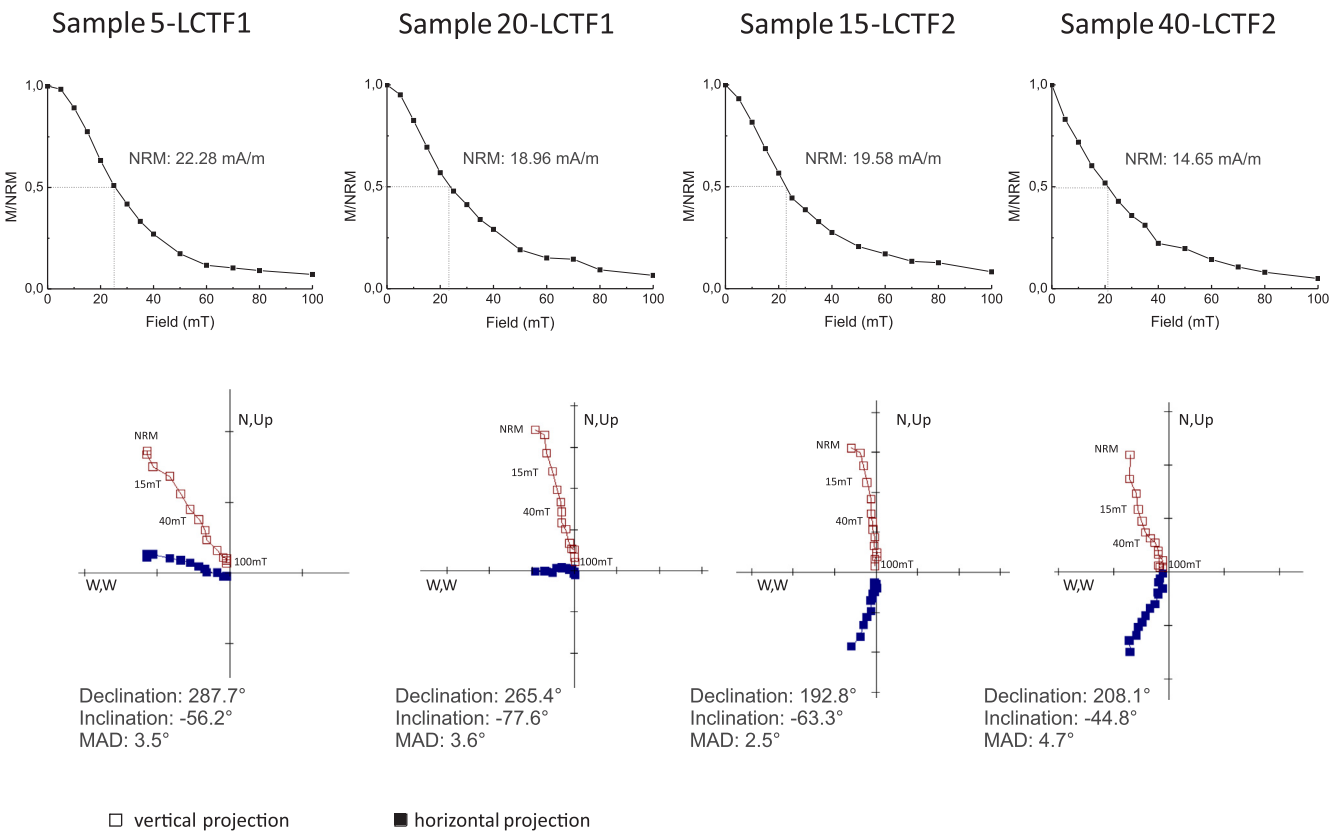

Fig. 8. Normalised intensity decay curves and orthogonal vector plots for four pilot samples from cores LTF1 and LCTF2, produced by stepwise AF demagnetisation at 5–10 mT steps, up to a maximum field of 100 mT. Closed blue (open red) circles denote the projection on the horizontal (vertical) plane. (For interpretation of the references to colour in this figure legend, the reader is referred to the web version of this article.)

minimum at app. 3450 cal years BP. Anyway, this minimum value should be taken with caution given that at that age there are data from a single record. From 3450 cal years BP to 1000 cal years BP, there is an oscillating pattern that repeats approximately every 400 years formed by a single isolated peak and two peaks together of approximately the same intensity. Declination exhibits an oscillating behaviour with

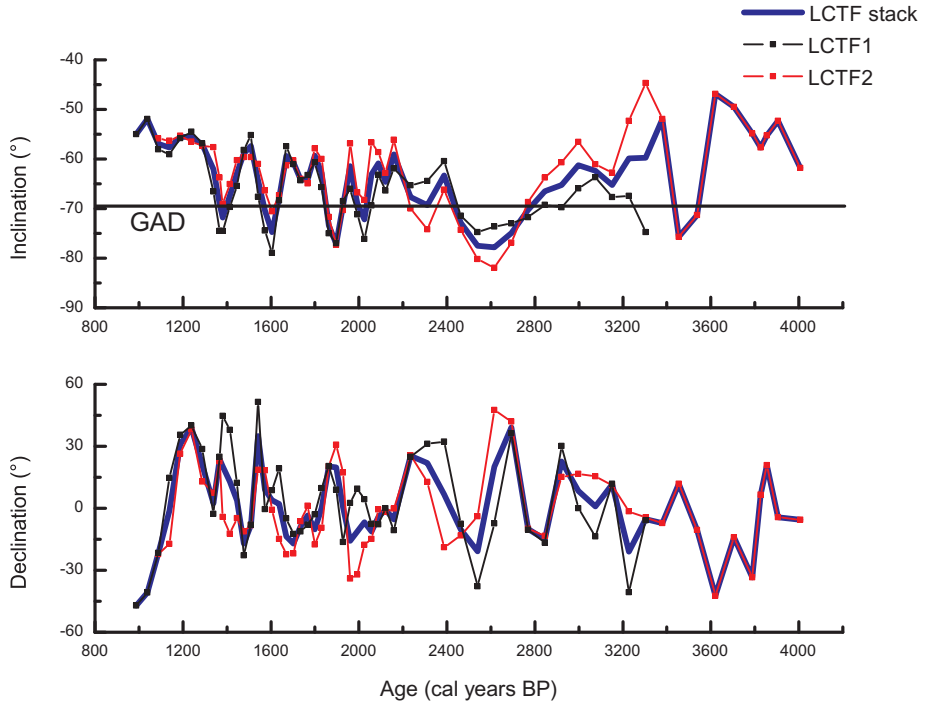

Fig. 9. Plots of inclination and declination for cores LCTF1 (black squares) and LCTF2 (red squares) and stacked profile (blue line). (For interpretation of the references to colour in this figure legend, the reader is referred to the web version of this article.)

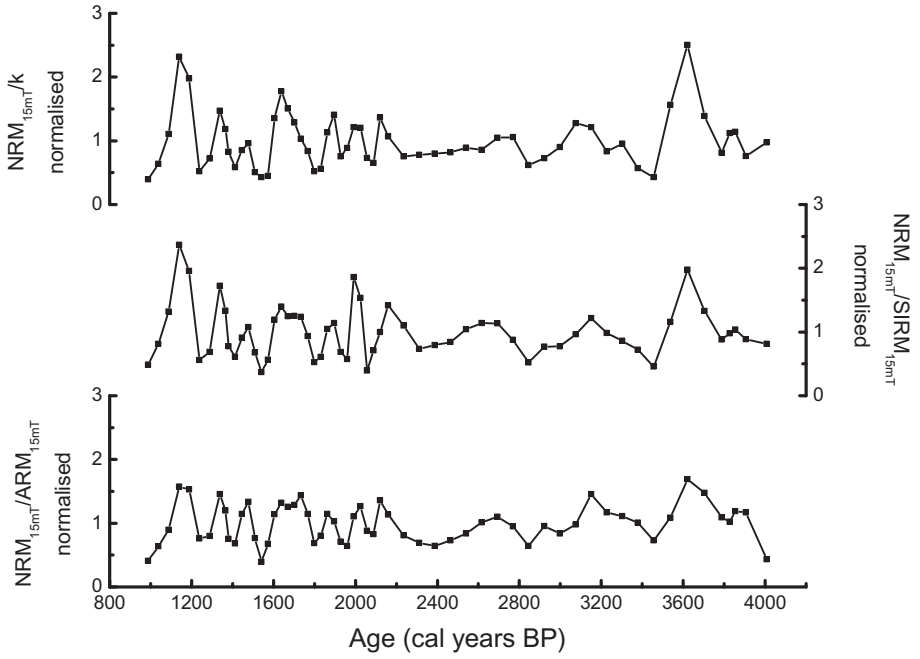

Fig. 10. Normalised estimates of relative paleointensity (RPI): NRM_{15mT}/k, $NRM_{15mT}/SIRM_{15mT}$ and NRM_{15mT}/ARM_{15mT} versus Age.

amplitude of app. ± 40° displaying extreme values at 3600, 2500 and 1000 cal years BP (minimum) and at 2700, 1580 and 1240 cal years BP (maximum) (Fig. 9). As shown in Fig. 9, the first two inclination and declination data correspond only to LCTF1. Because declination data show a large variation that could be doubtful and they are unsupported by LCTF2 data, we decided to remove these two declination data from the plot that shows the final results (Fig. 13). In this way, the resulting fluctuation in the first part of the declination record varies around 60°, which is also observed in previous studies (Lisé-Pronovost et al., 2013; Yang et al., 2012; Usapkar et al., 2016; among others).

5.5. Relative paleointensity records

Rock magnetic results attest that the sediments of Carmen Lake are suitable for constructing the RPI curves (Relative Paleointensity) (Tauxe, 1993), including the well-defined magnetisation component carried by pseudo-single domain (PSD) magnetite, and variations of less than a factor of 10 in the magnetic concentration. Estimation of RPI from sediments can be obtained by normalising the measured NRM by an appropriate magnetic parameter in order to compensate for the variable concentration of ferrimagnetic minerals (e.g., Tauxe, 1993). Concentration-dependent parameters such as ARM, IRM or k are generally employed as normalisers. Levi and Banerjee (1976) have proposed to derive RPI estimates from NRM and also ARM and SIRM after an AF demagnetisation treatment in order to discard viscous and other spurious magnetisation components of relatively low magnetic stability. After analysing AF demagnetization characteristics of NRM directions (Fig. 8) we chose the 15mT-level to quantify RPI estimates. There is a general consensus that if the three normalisation parameters yield similar profiles of relative paleointensity, then any one of the three parameters is a satisfactory normaliser. In order to compare the different paleointensity estimates, the stacked values of NRM_{15mT}/ARM_{15mT}, $NRM_{15mT}/SIRM_{15mT}$ and NRM_{15mT}/k were further normalised by dividing each value by their respective arithmetic means. The three RPI estimates produce similar results, but differ in amplitude of peaks at 1139, 1992 and 3621 cal years BP (Fig. 10). Slightly higher values of ARM/SIRM are observed in these levels (6, 56 and 104 cm, respectively) (Fig. 4), which would imply an increase in the proportion of finer grains, that is, the NRM_{15mT}/ARM_{15mT} decrease but the $NRM_{15mT}/SIRM_{15mT}$ increase.

In order to confirm that the normalised records are free of environmental influences, spectral analyses of normalised remanences, normalisation parameters and a coherence test were performed following the method of Tauxe and Wu (1990). Spectral analysis using the MCCLEAN algorithm (Heslop and Dekkers, 2002) and calculation of coherence spectra were performed using the MATLAB 6.1 software (Fig. 11). The cohere analysis further indicates that the normalised intensity curves are not coherent with normalisation parameters (no significant frequencies above the 95% confidence level), except for NRM_{15mT}/k that show coherence with its normaliser in a narrow frequency range (Fig. 11). Following Barletta et al. (2010) and the references therein, the choice of the appropriate normaliser can be performed using the remanence whose demagnetisation curve most closely resembles that of NRM. This can be assessed by comparing the AF coercivity spectra of NRM, ARM and SIRM. Coercivity spectra of the NRM and ARM are nearly identical, while that of the SIRM is much softer (Fig. 12). This behaviour was observed in most of the analysed pilot samples which were taken along the whole cores. We conclude that ARM_{15mT} is the most appropriate normaliser to construct the RPI proxies in these sediments.

6. Discussion

6.1. Pattern of paleosecular variation

To confirm the fidelity of the geomagnetic field records, we compare the stacked PSV curves obtained for cores LCTF1 and LCTF2, with the nearest available reference PSV curves (with a distance < 250 km) for Laguna Potrok Aike (51°58′S, 70°23′W; Gogorza et al., 2012) over the same time interval (Fig. 13). The lacustrine records from Escondido lake (about 41°S, 71°30′W; Gogorza et al., 2002) and El Trébol lake (41°04′S 71°29′W; Irurzun et al., 2006) were also included, although they are located at a distance of ~1500 km. The objective was to evaluate the similarity of the curves and analyse the possibility of constructing regional type curves in the future. Although records from Laguna Potrok Aike show more details because of the relatively higher depositional rates they show rather consistent patterns compared to the sediments of Carmen Lake. Following the strategy suggested by Yang

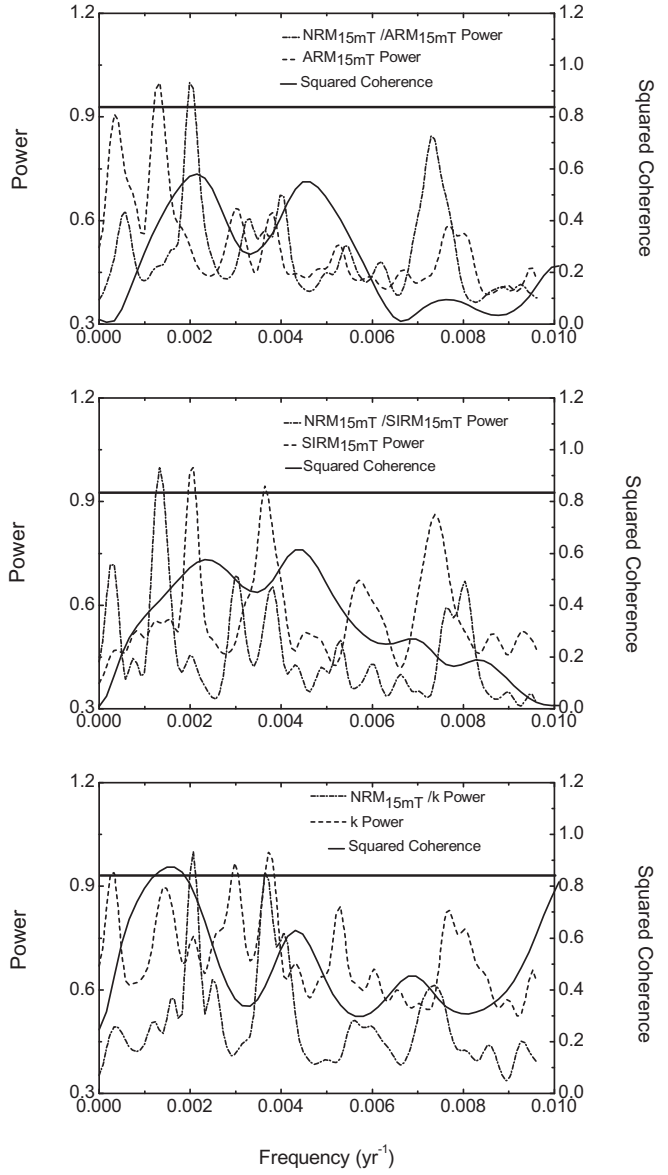

Fig. 11. Spectral analysis of three normalisation parameters (ARM_{15mT}, $SIRM_{15mT}$ and k) and three normalised remanences (NRM_{15mT}/ARM_{15mT}, $NRM_{15mT}/SIRM_{15mT}$ and NRM_{15mT}/k). Coherence tests of relative paleointensity curves with respect to the normalisation parameters, showing that the normalised intensity curves are generally not coherent with the normalisation parameters.

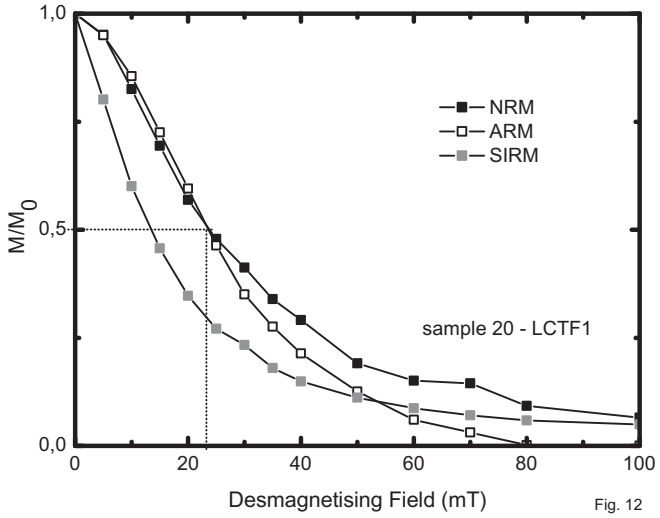

Fig. 12. Typical AF demagnetisation curves of Natural Remanent Magnetisation (NRM), Anhysteretic Remanent Magnetisation (ARM) and Saturation of the Isothermal Remanent Magnetisation (SIRM) for sample 20 (LCTF2).

et al. (2012), both inclination and declination was used to correlate the records synchronously because the geomagnetic field is vector.

The PSV record of Carmen Lake cores clearly shows the major maxima and minima in inclination and declination as seen in the other PSV records, indicating the same sources of the Earth's magnetic field variation. The curves were divided into five sectors (I–V) based on these main characteristics in order to visualize more clearly the coherence between the records. The paleomagnetic inclination and declination trends of Carmen Lake appear to match closely the Potrok Aike curves (Fig. 13), which is understandable and expected considering the proximity between both sites. However, a good correlation is also possible to perform with the lakes Escondido and El Trébol both located in northern Patagonia. In sector V (~4000–3450 cal years BP), a prominent westerly swing is observed in Carmen and Potrok Aike and it is shown smoother in the record of El Trébol; while the records of inclination are close for Potrok Aike and Carmen on the one hand and between Escondido and El Trébol on the other. Notably, a remarkable match is observed for the increasing trend in inclination at ~3450–2540 cal years BP (IV), shown by all records. Also, the records of declination show similar characteristics in lakes Escondido and El Trébol although in less detail. In sector III (~2540–2000 cal years BP), a large magnetic declination swing is observed at ~2500 cal BP in the records of Carmen Lake and Potrok Aike and less sharply in Escondido. This magnetic feature ("f-event") was previously noted in Northern lacustrine European PSV records by Turner and Thompson (1981). It has also been observed in two other PSV records from Icelandic lakes (Olafsdottir et al., 2009) and in high-resolution marine records from eastern Canada (Barletta et al., 2008). From ~2000 to 1400 and 1400–1000 cal years BP, we can only compare the records of Carmen Lake with the data of Escondido Lake. Although it is possible to observe similar swings in both records, it is obvious that the variations in Carmen Lake are higher.

The inaccuracies in dating methods could explain the small discrepancies in timing observed between Carmen Lake and the other records. Besides, it is possible to confirm the conclusions found in previous works (Gogorza et al., 2012), that the overall consistency of PSV patterns among these records suggests that these features are common for Southern Argentina. These coeval features also suggest that PSV can provide a useful tool for stratigraphic correlation on a regional scale.

6.2. Pattern of RPI variation

In order to compare, the following RPI records were displayed: WEGA (65°S) (Macri et al., 2005), Larsen-A Ice Shelf (64°S) (Brachfeld et al., 2003), Esmeralda (61°S) (Irurzun et al., 2017), Potrok Aike (52°S) (Gogorza et al., 2012), Escondido (Gogorza et al., 2004) and El Trébol (41°S) (Gogorza et al., 2006) divided into the same sectors as inclination and declination (Fig. 14). A series of intensity high can be identified in the records from the Southern Hemisphere. In particular, a close correlation is observed in the records of Carmen and Potrok Aike, except in the period ~2800–3500 cal years BP, in which a notable high (3150 cal years BP) is displayed in all records except in Potrok Aike. This discrepancy could be explained by the fact that the record of Potrok Aike could be affected by changes in the magnetic grain size not corrected by the normalisations. All the records generally agree in sector V (~4000–3450 cal years BP). In particular, two peaks appear clearly defined in Carmen, Potrok Aike and Esmeralda. In the period ~3450–2540 cal years BP (IV), there is a good coincidence between the

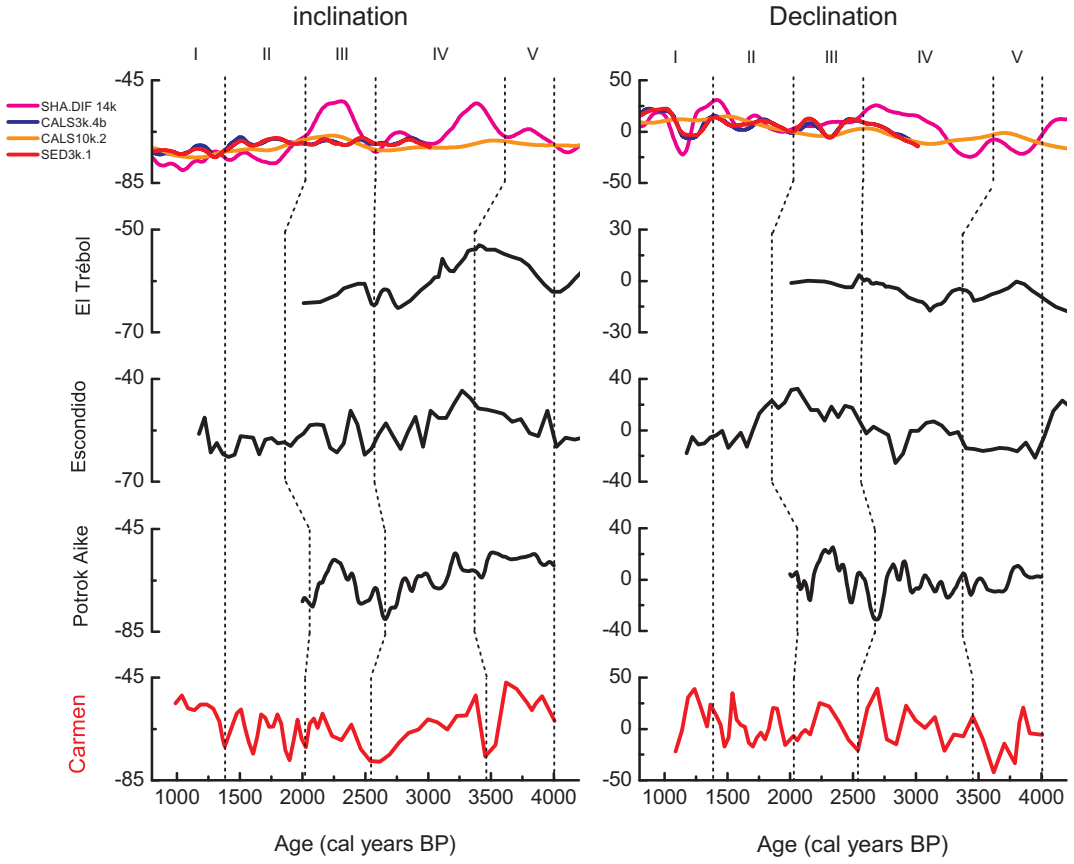

Fig. 13. Stacked inclination and declination logs from Carmen Lake, in previous work (Gogorza et al., 2002, 2004, 2012; Irurzun et al., 2006) as a function of age and SED3k.1 (Korte et al., 2009), CALS3k.4b (Korte and Constable, 2011), CALS10k.2 (Brown et al., 2015; Constable et al., 2016) and SHA.DIF.14k (Pavón Carrasco et al., 2014) outputs.

records of Carmen Lake, WEGA, Escondido and El Trébol, including a good temporal agreement. In sector III (~2540–2000 cal years BP), there is discrepancy in the different records, although the records of Carmen Lake shows a remarkable agreement with WEGA. In sector II (~2000–1400 cal years BP), Carmen, Esmeralda and Larsen lakes display a maximum (~1700 cal years BP), although the resolution is different. Finally, in the period ~1400–1000 cal years BP, two peaks are observed in Carmen Lake (1340 and 1140 cal years BP) and they are barely suggested in Esmeralda and WEGA. In general, many centennial RPI features can be clearly correlated, within the dating uncertainties, among the records suggesting a common geomagnetic origin.

6.3. Comparison with models

Declination and inclination records from Carmen Lake are plotted together with the predictions from the global models provided by GeoMagia50 database (2017) (CALS3K.4b (Korte and Constable, 2011), CALS10k.2 (Brown et al., 2015); (Constable et al., 2016), SED3k.1 (Korte et al., 2009)) and SHA.DIF.14 (Pavón Carrasco et al., 2014) (Fig. 13). These models are the latest developed using all the available paleomagnetic data for their corresponding time intervals, applying the spherical harmonic analysis in space and the penalised cubic B splines in time. SHA.DIF.14 is only based on archeomagnetic data (including lava flow data), while CALS3K.4b and CALS10k.2 also include lake sediment data. The latter model is aimed to provide a robust representation of the large scale field at the core-mantle boundary, but the SHA.DIF.14 model provides more variability in terms of both spatial and temporal resolution (Pavón Carrasco et al., 2014; Goguitchaichvili et al., 2015). In agreement with Goguitchaichvili et al. (2015), SHA.DIF.14 presents a clear improvement in field resolution with respect to other current models of the geomagnetic field for the Holocene. In both declination and inclination, the agreement observed between this model and our records has improved significantly with respect to previous models. In particular, it is interesting to observe the concordance in the amplitude of the variations, which was not taken into account in the extremely smoothed previous models. In particular, the "f-event" is also quite well reproduced by SHA.DIF.14. Finally, SED3k.1 is constructed using all available sediment data from the Southern Hemisphere (Donadini et al., 2009), including records from Lake El Trébol (Gogorza et al., 2006) and Escondido (Gogorza et al., 2002, 2004). The data have a better global distribution (less biased towards the Northern Hemisphere) than previous models and can be used for prediction in the Southern Hemisphere (Korte et al., 2009). In any event, the Southern Hemisphere is very poorly sampled, contributing with only 3% of the data (Donadini et al., 2009). As shown in Fig. 13, the model output is smooth and it does not take into account the variability observed in the records of Carmen Lake, not even in Lake El Trébol and Escondido whose data were used to develop the model. Therefore, these significant differences could imply the presence of distinctive and different geomagnetic features originating from non-dipolar or even particular hemispheric sources which prevent a correlation with these models, in which Southern Hemisphere is very poorly represented.

When RPI records are compared with the models, it is observed that a better although limited agreement is obtained with SHA.DIF.14. It is not surprising to observe these differences between them because our data are local records but the predicted values come from a global comprehensive model. Some local effects from non-dipole field would unavoidably be involved in our local records even if the effects were minor. Besides, because very few paleomagnetic data from the Southern

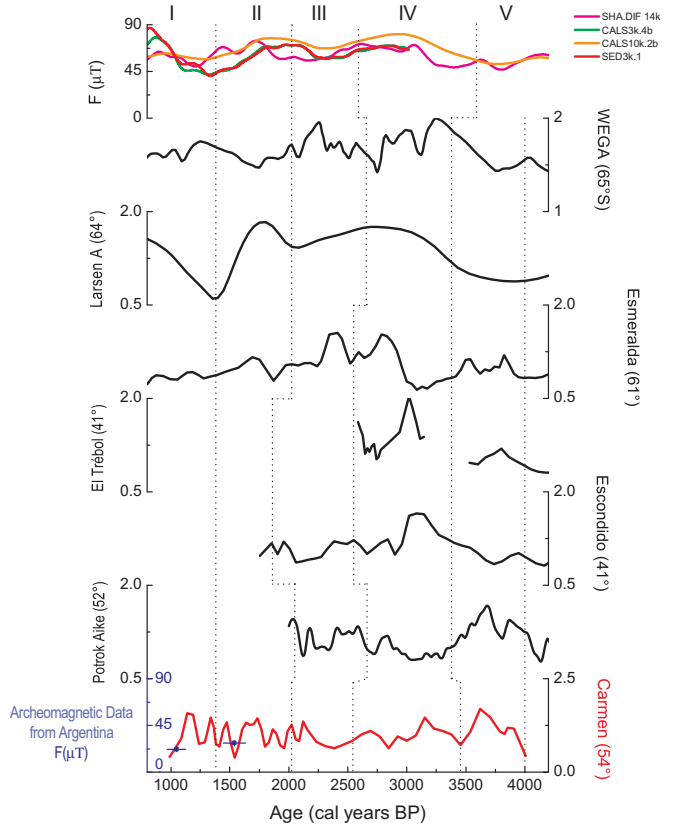

Fig. 14. Comparison of normalised intensity record from Carmen Lake with relative paleointensity records from WEGA (65°S) (Macri et al., 2005), Larsen-A Ice Shelf (64°S) (Brachfeld et al., 2003), Esmeralda Lake (61°S) (Irurzun et al., 2017), Laguna Potrok Aike (52°S) (Gogorza et al., 2012), Escondido Lake (Gogorza et al., 2004), El Trébol Lake (41°S) (Gogorza et al., 2006) and the models SED3k.1 (Korte et al., 2009), CALS3k.4b (Korte and Constable, 2011), CALS10k.2 (Brown et al., 2015; Constable et al., 2016) and SHA.DIF.14k (Pavón Carrasco et al., 2014). Two archeointensity determinations from Argentina (blue squares) available for the studied period (Goguitchaichvili et al., 2012) are plotted along the RPI curve from Carmen Lake. (For interpretation of the references to colour in this figure legend, the reader is referred to the web version of this article.)

Hemisphere has been contributed to the models, the local prediction with fewer constraints might show less confidence in this area.

6.4. Comparison with archeomagnetic records

The number of reliable archeointensity determinations obtained from Argentina for the past millennium remains limited (Goguitchaichvili et al., 2011, 2012, 2015). Moreover, only two archeointensity determinations are available for the studied period (Goguitchaichvili et al., 2012). The pottery samples analysed were recovered at two archaeological sites (Túmulo de Campana and La Bellaca) located in a small area of the wetlands of the lower Paraná, within a geographical range of 50 km. This area is situated in the central-eastern sector of the Pampean region (Argentina) on parallel 34°SL (Goguitchaichvili et al., 2012). Both archeointensity records are plotted together with the data from Carmen Lake (Fig. 14; blue square). In order to compare them, the archeointensity determinations are plotted in the same scale used to plot the models output. The scope of this analysis is obviously limited because both records are located more than 2500 km apart and that data from Carmen Lake are relative paleointensity data. Despite this, a good agreement is observed. Some discrepancies in age offsets may be related to dating problems and different time-lags of Detrital Remanent Magnetisation acquisition in the sediments (Ali et al., 1999; Yang, 2009) .

7. Conclusions

We present a high resolution paleomagnetic secular variation and relative paleointensity stack for the period 1000–4000 cal years BP recorded in two sediment cores from Carmen Lake. The remanence is carried by Titanomagnetite with a grain size of ~8–16 μm while the mineral concentration varies between 0.01 and 0.09%. Secular variations of the geomagnetic field derived from Carmen Lake show a generally consistent pattern with other records within the age dating uncertainties. Especially, a series of peaks and lows have been clearly defined in the inclination and declination and also in the RPI curves in the studied period. The simultaneousness of the main geomagnetic features over wide areas throughout the South Western Hemisphere, within the errors of the different chronologies for different sites, supports the fidelity of the individual PSV records. The good coincidence between the records provides a promising approach to refining the chronology of the sediments and encourages us to deduce the general pattern for Southern of South America.

Acknowledgements

Laboratory tasks were supported by the Comisión Nacional de Investigaciones Científicas y Técnicas de la República Argentina (CONICET – Argentina) PIP 112-200801-01161 and PIP 112-201201-00573 (CONICET), Agencia Nacional de Promoción Científica y Tecnológica (ANPCyT – Argentina) PICT 21012-0628, Universidad de Buenos Aires (UBA) and Universidad Nacional del Centro de la Provincia de Buenos Aires (UNCPBA). We would like to thank C. Laprida and N. García Chapori for their collaboration in the field work. We are much indebted to Pablo Zubeldía for assistance with measurements. The authors are grateful for valuable and helpful comments and suggestions from two anonymous referees.

References

Ali, M., Oda, H., Hayashida, A., Takemura, K., Torii, M., 1999. Holocene paleomagnetic secular variation at Lake Biwa, central Japan. Geophys. J. Int. 136, 218–228.
Anker, S.A., Colhoun, E.A., Barton, C.E., Peterson, M., Barbetti, M., 2001. Holocene vegetation and palaeoclimatic and Paleomagnetic history from Lake Johnston, Tasmania. Quat. Res. 56, 264–274.
Bailey, M.E., Dunlop, D.J., 1983. Alternating field characteristics of pseudo-single-domain (2–14 μm) and multidomain magnetite. Earth Planet. Sci. Lett. 63, 335–352.
Barletta, F., St-Onge, G., Channell, J.E.T., Rochon, A., Polyak, L., Darby, D.A., 2008. High resolution paleomagnetic secular variation and relative paleointensity records from the western Canadian Arctic: implication for Holocene stratigraphy and geomagnetic field behaviour. Can. J. Earth Sci. 45, 1265–1281.
Barletta, F., St-Onge, G., Channell, J.E.T., Rochon, A., 2010. Dating of Holocene western Canadian Arctic sediments by matching paleomagnetic secular variation to a geomagnetic field model. Quat. Sci. Rev. 29 (17–18), 2315–2324.
Bleil, U., Dillon, M., 2008. Holocene Earth's magnetic field variations recorded in marine sediments of the NW African continental margin. Stud. Geophys. Geod. 52, 133–155.
Bloemendal, J., Lamb, B., King, J., 1988. Paleoenvironmental implications of rock-magnetic properties of late Quaternary sediment cores from the eastern equatorial Atlantic. Paleoceanography 3, 61–87.
Brachfeld, S.A., Domack, E., Kisel, C., Laj, C., Leventer, A., Ishman, S., Gilbert, R., Camerlenghi, A., Eglinton, L.B., 2003. Holocene history of the Larsen-A Ice Shelf constrained by geomagnetic paleointensity dating. Geology 31 (9), 749–752.
Bronk Ramsey, C., 1995. Radiocarbon calibration and analysis of stratigraphy: the OxCal program. Radiocarbon 37 (2), 425–430.
Bronk Ramsey, C., 2008. Deposition models for chronological records. Quat. Sci. Rev. 27 (1–2), 42–60.
Bronk Ramsey, C., Lee, S., 2013. Recent and planned developments of the program OxCal. Radiocarbon 55 (2–3), 720–730.
Brown, M.C., Donadini, F., Nilsson, A., Panovska, S., Frank, U., Korhonen, K., Schuberth, M., Korte, M., Constable, C.G., 2015. GEOMAGIA50.v3: 2. A new paleomagnetic database for lake and marine sediments. Earth Planets Space 67. http://dx.doi.org/10.1186/s40623-015-0233-z.
Constable, C., Korte, M., Panovska, S., 2016. Persistent high paleosecular variation activity in Southern hemisphere for at least 10 000 years. Earth Planet. Sci. Lett. 453, 78–86.
Coronato, A., Ponce, J.F., Quiroga, D., Gogorza, C.S.G., 2017. Emplazamiento geológico-

geomorfológico de Carmen Lake, estepa fueguina, Argentina. Registro sedimentario del Holoceno Tardío. Rev. Asoc. Geol. Argentina (in press).
Creer, K.M., Tucholka, P., 1982. Secular variation as recorder in lake sediments: a discussion of North American and European results. Philos. Trans. R. Soc. Lond. A 306, 87–102.
Day, R., Fuller, M., Schmidt, V.A., 1977. Hysteresis properties of titanomagnetites: grain size and composition dependence. Phys. Earth Planet. Inter. 13, 260–267.
Dearing, J.A., 1999. Environmental Magnetic Susceptibility: Using the Bartington MS2 System. Chi Pub., Kenilworth, pp. 54.
Donadini, F., Korte, M., Constable, C.G., 2009. Geomagnetic field for 0–3 ka: 1. New data sets for global modeling. Geochem. Geophys. Geosyst. 10 (6), Q06007.
Dunlop, D.J., 2002. Theory and application of the Day plot (Mrs/M versus Hcr/Hc): 2. Application to data for rocks, sediments and soils. J. Geophys. Res. 107 (B3), 2057.
Dunlop, D.J., Özdemir, Ö., 1997. Rock Magnetism, Fundamentals and Frontiers. Cambridge Univ. Press, Cambridge, U. K.
Evans, M., Heller, F., 2003. In: Environmental Magnetism. Principles and Applications of Enviromagnetics. Academic Press, Elsevier, pp. 317.
Frank, U., Nowaczyk, N.R., Negendank, J.F.W., Melles, M., 2002. A paleomagnetic record from Lake Lama, northern Central Siberia. Phys. Earth and Planet. Int. 133, 3–20.
GeoMagia50 database last access July, 2017. http://geomagia.gfz-potsdam.de.
Gogorza, C.S.G., Sinito, A.M., Lirio, J.M., Nuñez, H., Chaparro, M., Vilas, J.F., 2002. Paleosecular variations 0–19,000 years recorded by sediments from Escondido Lake (Argentina). Phys. Earth Planet. Int. 133, 35–55.
Gogorza, C.S.G., Lirio, J.M., Nuñez, H., Chaparro, M.A.E., Bertorello, H.R., Sinito, A.M., 2004. Paleointensity studies on Holocene-Pleistocene sediments from lake Escondido, Argentina. Phys. Earth Planet. Int. 145, 219–238.
Gogorza, C.S.G., Irurzun, M.A., Chaparro, M.A.E., Lirio, J.M., Nuñez, H., Bercoff, P.G., Sinito, A.M., 2006. Relative paleointensity of the geomagnetic field over the last 21,000 cal years BP from sediment cores, Lake El Trébol (Patagonia, Argentina). Earth Planets Space 58, 1323–1332.
Gogorza, C.S.G., Sinito, A.M., Ohlendorf, C., Kastner, S., Zolitschka, B., 2011. Paleosecular variation and paleointensity records for the last millennium from southern South America (Laguna Potrok Aike, Santa Cruz, Argentina). Phys. Earth Planet. Int. 184, 41–50.
Gogorza, C.S.G., Irurzun, M.A., Sinito, A.M., Lisé-Pronovost, A., St-Onge, G., Haberzettl, T., Ohlendorf, C., Kastner, S., Zolitschka, B., 2012. High-resolution paleomagnetic records from Laguna Potrok Aike (Patagonia, Argentina) for the last 16,000 years. Geochem. Geophys. Geosyst. 13, 12.
Goguitchaichvili, A., Greco, C., Morales, J., 2011. Geomagnetic field intensity behavior in South America between 400 AD and 1800 AD: first archeointensity results from Argentina. Phys. Earth Planet. Int. 186, 191–197.
Goguitchaichvili, A., Loponte, D., Morales, J., Acosta, A., 2012. The archaeointensity of the rarth's magnetic field retrieved from Pampean ceramics (South America). Archaeometry 54 (2), 388–400.
Goguitchaichvili, A., Morales, J., Schavelzon, D., Vásquez, C., Gogorza, C., Loponte, D., Rapalini, A., 2015. Variation of the Earth's magnetic field strength in South America during the last two millennia: new results from historical buildings of Buenos Aires and Re-evaluation of regional data. Phys. Earth Planet. Int. 245, 15–25.
Heil, C.W., Jr., King, J.W., Rosenbaum, J.G., Reynolds, R.L., Colman, S.M., 2009. Paleomagnetism and environmental magnetism of GLAD800 sediment cores from Bear Lake, Utah and Idaho. In: Rosenbaum, J.G., Kaufman D.S., (Eds.). Paleoenvironments of Bear Lake, Utah and Idaho, and its Catchment: Geological Society of America Special 450. pp. 291–310. doi: 10.1130/2009.2450(13).
Heslop, D., Dekkers, M., 2002. Spectral analysis of unevenly spaced time series using CLEAN: signal recovery and derivation of significance levels using a Monte Carlo simulation. Phys. Earth Planet. Inter. 130, 103–116. http://dx.doi.org/10.1016/S0031-9201(01)00310-7.
Holme, R., Olsen, N., 2006. Core surface flow modelling from high-resolution secular variation. Geophys. J. Int. 166, 518–528.
Irurzun, M.A., Gogorza, C.S.G., Sinito, A.M., Lirio, J.M., Nuñez, H., Chaparro, M.A.E., 2006. Paleosecular variations recorded by sediments from Lake El Trébol, Argentina. Phys. Earth Planet. Int. 154, 1–17.
Irurzun, M.A., Chaparro, M.A.E., Sinito, A.M., Gogorza, C.S.G., Nuñez, H., Nowaczyk, N.R., Böhnel, H.N., 2017. Relative palaeointensity and reservoir effect on Lake Esmeralda, Antarctica. Antarct. Sci. 29 (4), 356–368.
Kirschvink, J.L., 1980. The least-squares line and plane and the analysis of paleomagnetic data. Geophys. J. Int. 62, 699–718.
Korte, M., Constable, C., 2011. Improving geomagnetic field reconstructions for 0–3ka. Phys. Earth Planet. Int. 188, 247–259.
Korte, M., Donadini, F., Constable, C.G., 2009. Geomagnetic field for 0–3 ka: 2. A new series of time-varying global models. Geochem. Geophys. Geosyst. 10, Q06008.
Lattard, D., Engelmann, R., Kontny, A., Sauerzapf, U., 2006. Curie temperatures of synthetic titanomagnetites in the Fe-Ti-O system: effects of composition, crystal chemistry, and thermomagnetic methods. J. Geophys. Res. 111, B12S28.
Levi, S., Banerjee, S.K., 1976. On the possibility of obtaining relative paleointensities from lake sediments. Earth Planet. Sci. Lett. 29, 219–226.
Lisé-Pronovost, A., St-Onge, G., Gogorza, C., Haberzettl, T., Preda, M., Kliem, P., Francus, P., Zolitschka, B., 2013. High-resolution paleomagnetic secular variations and relative paleointensity since the Late Pleistocene in southern South America. Quat. Sci. Rev. 71, 91–108.
Macri, P., Sagnotti, L., Dinares-Turell, J., Caburlotto, A., 2005. A composite record of Late Pleistocene relative geomagnetic paleointensity from the Wilkes Land Basin (Antarctica). Phys. Earth Planet. Int. 151, 223–242.
Merrill, R.T., Mc Elhinny, M.W., 1983. The earth's magnetic field. Its history, origin and planetary perspective. In: Donn, W.L. (Ed.), International Geophysics Series. Academic Press Inc.
Moreno, A., Cacho, I., Canals, M., Prins, M.A., Sánchez-Goñi, M.F., Grimalt, J.O., Weltje, G.J., 2002. Saharan dust transport and high latitude climatic variability: the Alboran Sea record. Quatern. Res. 58, 318–328.
Nourgaliev, D.K., Heller, F., Borisov, A.S., Hajdas, I., Bonani, G., Iassonov, P.G., Oberhänsli, H., 2003. Very high resolution paleosecular variation record for the last ~1200 years from the Aral Sea. Geophys. Res. Lett. 30 (17), 1914. http://dx.doi.org/10.1029/2003GL018145.
Olafsdottir, S., Stoner, J.S., Geirstottir, A., 2009. High-resolution Holocene Paleomagnetic Secular Variation Records from Iceland: Marine–Terrestrial Synchronization. GSA Annual Meeting, Abstract volume.
Olsen, N., Hulot, G., Sabaka, T.J., 2010. Sources of the geomagnetic field and the modern data that enable their investigation. In: Freeden, W., Nashed, M.Z., Sonar, T. (Eds.), Handbook of Geomathematics. Springer-Verlag, Berlin Heidelberg, pp. 105–124.
Oxcal 4.2 calibration software last access March, 2017. https://c14.arch.ox.ac.uk.
Pavón Carrasco, F.J., Rodríguez-González, J., Osete, M.L., Torta, J.M., 2014. A Matlab tool for archaeomagnetic dating. J. Archaeol. Sci. 38, 408–419.
Prévot, M., Mankinen, E.A., Grommé, S., 1983. High paleointensities of the geomagnetic field from thermomagnetic studies on Rift Valley pillow basalts from the Mid-Atlantic Ridge. J. Geophys. Res. 88 (B3), 2316–2326.
Stoner, J.S., Jennings, A., Kristjánsdóttir, G.B., Dunhill, G., Andrews, J.T., Hardardottir, J., 2007. A paleomagnetic approach toward refining Holocene radiocarbon-based chronologies: paleoceanographic records from the north Iceland (MD99-2269) and east Greenland (MD99-2322) margins. Paleoceanography 22.
St-Onge, G., Stoner, J.S., Hillaire-Marcel, C., 2003. Holocene paleomagnetic records from the St. Lawrence Estuary, eastern Canada: centennial- to millennial-scale geomagnetic modulation of cosmogenic isotopes. Earth Planet. Sci. Lett. 209, 113–130.
Tauxe, L., 1993. Sedimentary records of relative paleointensities of the geomagnetic field: theory and practice. Rev. Geophys. 31, 319–354. http://dx.doi.org/10.1029/93RG01771.
Tauxe, L., Wu, G., 1990. Normalised remanence in sediments of the western equatorial Pacific: relatively intensity of the geomagnetic field? J. Geophys. Res. 95, 12337–12350.
Tauxe, L., Mullender, T.A.T., Pick, T., 1996. Potbellies, wasp-waists, and superparamagnetism in magnetic hysteresis. J. Geophys. Res. 101 (B1), 571–583.
Thompson, R., Oldfield, F., 1986. In: Environmental Magnetism. Allen & Unwin Ltd, pp. 225.
Turner, G.M., Thompson, R., 1981. Lake sediment record of the geomagnetic secular variation in Britain during Holocene times. Geophys. J. R. Astron. Soc. 65 (3), 703–725.
Usapkar, A., Dewangan, P., Badesab, F., Mazumdar, A., Ramprasad, T., Krishna, K.S., Basavaiah, N., 2016. High resolution Holocene paleomagnetic secular variation records from Bay of Bengal. Phys. Earth Planet. Inter. 252, 49–76.
Yang, X., Heller, F.B., Yang, J., Su, Z., 2009. Paleosecular variations since ~9000 yr BP as recorded by sediments from maar lake Shuangchiling, Hainan, South China. Earth Planet. Sci. Lett. 209, 113–130.
Yang, X.Q., Liu, Q.S., Duan, Z.Q., Su, Z.H., Wei, G.J., Jia, G.D., Ouyang, T.P., Su, Y.L., Xie, L.H., 2012. A Holocene Paleomagnetic secular variation record from Huguangyan maar Lake, southern China. Geophys. J. Int. 190 (1), 188–200.
Yang, X.Q., Yang, J., Su, Z., Huang, W., Wang, J., 2013. Paleosecular variations refining the chronology of the sediments from the Pearl River Delta, southern China. Holocene 23 (5), 635–644.